

## Research Paper

## Numerical study on initiation of oblique detonation wave by hot jet

Aifeng Wang<sup>a</sup>, Jing Bian<sup>b,\*</sup>, Honghui Teng<sup>b</sup><sup>a</sup> Aero Engine Academy of China, Aero Engine Corporation of China, Beijing 101304, China<sup>b</sup> School of Aerospace Engineering, Beijing Institute of Technology, Beijing 100081, China

## ARTICLE INFO

## Keywords:

Oblique detonation  
Hot jet  
Hydrogen  
Initiation length

## ABSTRACT

Reliable detonation initiation is critical in detonation engines, especially for oblique detonation engines covering a wide range of flight regimes. The widely-studied oblique shock initiation usually leads to a significant variation in initiation length, making it difficult to adapt to the wide range of flight conditions. In this study, hot jets in the induction zone, i.e. behind the oblique shock, are introduced to explore the possibility of jet initiation, providing a potential method for initiation control. Results show that hot jet can decrease the initiation length to achieve rapid initiation and change the wave structure simultaneously, which is attributed to the oblique shock induced by a gaseous wedge. Thermal analyses of jet-initiated ODWs are also conducted through total pressure recovery. Results indicate that jet-initiated ODWs have a slightly better total pressure recovery than the original ODW. Furthermore, the jet angle and position are varied to analyze their effects on the initiation position, which is insensitive to the former while sensitive to the latter. A large jet angle may lead to a strong solution of secondary oblique detonation, which has not been previously reported.

## 1. Introduction

Detonation is a pressure-gain combustion process with heat release occurring in a shock-induced high-pressure state, facilitating its application in propulsion systems [1,2]. In recent decades, three detonation engine types have been proposed and investigated: these are named the pulse [3–5], rotating [6–8], and oblique detonation engines [9–12]. Among these, the oblique detonation engine (ODE) is a type of air-breathing ramjet engine suitable for hypersonic aircraft. However, oblique detonation waves (ODWs) inside the engine involve complex initiation structures, so it is necessary to investigate the initiation mechanisms and propose proper initiation methods.

ODW initiation can be viewed as a transition from oblique shock to oblique detonation, and the transition type might be abrupt or smooth [13–15]. Previous studies [16,17] have frequently used the ideal initiation by a semi-infinite wedge to investigate the ODW initiation mechanism. Furthermore, ODWs triggered by a cone [18], blunt wedge, [19] or double wedge [20–22] have been simulated to study more complicated but controllable initiation methods. Because of the difficulty in generating high-speed inflow, hypersonic projectiles such as spherical [23,24] and conical projectiles [25] have been widely applied to initiate ODWs experimentally. With the advancement of wind tunnel technology, Zhang et al. [26] showed the stability of an ODW through the JF-12

wind tunnel, further verifying the feasibility of ODEs for hypersonic propulsion.

ODW initiation inside a hypersonic engine is different and more complicated than the ideal ODWs studied above. The inflow parameters depend on the flight regime of the aircraft, which cannot be adjusted freely. Recent studies [27,28] have demonstrated that both the wave structures of the initiation region and the initiation lengths vary significantly, so spontaneous initiation through an oblique shock is not applicable because of the limited space of the combustor. Triggering ODWs using a hot jet is a potential solution for realistic initiation in the combustor. Li et al. [29] introduced a transverse hot jet to the induction zone for the first time. Jet-controlled ODWs are simulated with a two-step chemical reaction model, demonstrating the potential of using a hot jet to adjust the height and initiation position of ODWs. Qin and Zhang [30] numerically studied ODWs initiated by a co-flow hot jet, showing that it can effectively shorten the initiation length compared with a straight wedge. The inlet introducing the co-flow jet might lead to a more complicated wave structure, which may add some complexity to practical applications. However, there has been no clear study of how ODWs with different initiation structures respond to a hot jet. Furthermore, the effects of a hot jet on wave stability and combustion efficiency are also yet to be clarified. This study adopts more realistic models (the chemical reaction model and sonic injector model described in Sec. 2) and more jet parameters to provide reference conclusions for practical

\* Corresponding author.

E-mail address: [bianjing2008@163.com](mailto:bianjing2008@163.com) (J. Bian).

Nomenclature	
$H_1$	Flight altitude
$K$	Jet position parameter
$L_{tp}$	Position of three wave point
$L_{in}$	Initiation length
$d$	Jet width
$M_1$	Flight Mach number
$p$	Pressure
$p_{st}$	Stagnation pressure
$p_w$	Pressure on the induction zone
$p_{cr}$	Sonic injection critical pressure
$p_i$	Injection pressure
$T$	Temperature
$T_{st}$	Stagnation temperature
$\sigma$	Total pressure recovery
$T_{cr}$	Sonic injection critical temperature
$T_i$	Injection temperature
$v$	Velocity
$v_i$	Injection velocity
$\beta_1$	Angle of OSW1
$\beta_2$	Angle of OSW2
$\varphi$	Flow deflection angle
$\theta_1$	Wedge angle
$\theta_2$	Gaseous wedge angle
$\delta$	Jet angle
$\gamma$	Specific heat ratio
ODW	Oblique detonation wave
OSW1	Oblique shock induced by wedge
OSW2	Oblique shock induced by gaseous wedge

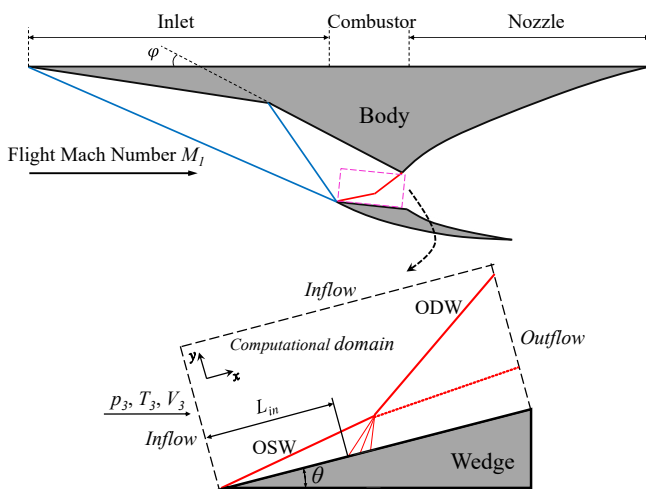


Fig. 1. Schematics of an oblique detonation engine and the computational domain of a wedge-induced ODW.

application.

This study examines jet initiation of an ODW inside a model engine, focusing on whether it is possible to control the initiation position with a wall hot jet. A transverse jet composed of detonation products is injected into the induction zone by sonic injection model, allowing investigation of the jet's effects on various ODWs. The numerical results show that a hot jet can decrease the initiation length to achieve rapid ODW initiation. The initiation mechanisms of jet-induced ODWs are revealed by

gaseous wedge analysis. Meanwhile, the effect of a hot jet on ODW combustion efficiency is also evaluated through total pressure recovery. In addition, the jet angle and position are varied to investigate their effects on initiation. The results indicate that ODWs are insensitive to jet angle but sensitive to jet position.

## 2. Physical and mathematical models

### 2.1. Physical models

A schematic of an ODE and the computational settings for a wedge-induced ODW are provided in Fig. 1. The engine inlet wave configuration adopts an equal-strength shock compression model, following many previous studies [27,28,31]. Two equal-strength shocks are used to slow and pressurize hypersonic air inflow at high flight altitudes. The fuel and air are assumed to be premixed well at the inlet. Sufficiently and quickly mixing hydrogen and air is critical for practical application of an ODE, as investigated by Zhang et al. [32]. However, injection of fuel with supersonic flow might lead to many complications [33]. To focus on the effects of a hot jet on ODW initiation, we assume the hydrogen and air are still premixed well before detonation. After the compression process, the supersonic homogeneous mixture reflects on the two-dimensional wedge to generate an oblique shock wave (OSW), leading to a high post-shock temperature that triggers rapid exothermic chemical reactions. The distance to the location where the local temperature reaches 110% of the post-shock temperature is defined as the numerical initiation length  $L_{in}$ , following many previous studies [34,35]. The rectangular dashed box in Fig. 1 represents the computational domain without jet control.

A schematic showing the computational settings and sonic injector model is provided in Fig. 2. The jet gases injected into the induction zone

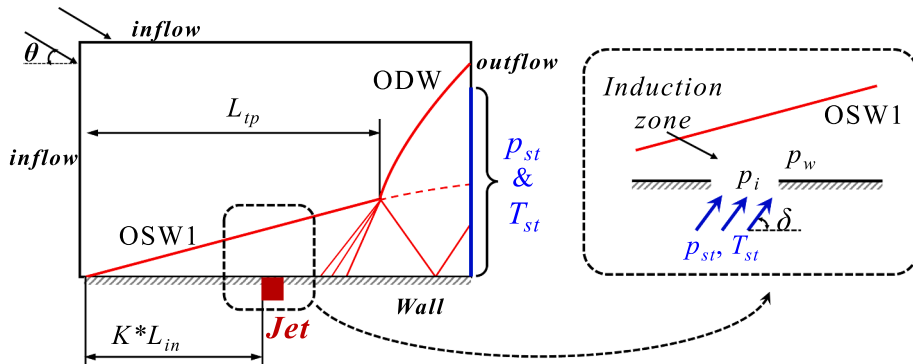


Fig. 2. Schematic of ODW initiation by a hot jet and the sonic injector model.

**Table 1**  
Simulation parameters for all presented cases.

Parameters	Values
$\varphi$	24°
$\theta_1$	19°
$d$ (mm)	2
$H_1$ (km)	30
$M_1$	8.0, 8.5, 9.0, 9.5
$K$	0.2, 0.4, 0.6, 0.8, 1.0, 1.2
$\delta$	10°, 30°, 50°, 70°, 90°

are detonation products. Because ODEs do not have the ability to self-start at low Mach numbers in practical application, the ODE is generally integrated with other engines as a combined power vehicle. Therefore, the hot jet can be created by a combined engine system such as a rotating detonation engine. The jet parameters are determined by the average total pressure  $p_{st}$  and total temperature  $T_{st}$  of the ODW outlet section, whose height is twice the initiation region height, as shown by the blue line in Fig. 2. Following many previous studies on detonation engines [36–38], the gas jets are injected using the sonic injection model [36] with jet inflow conditions ( $p_i$ ,  $T_i$ ,  $v_i$ ) computed assuming isentropic conditions through a convergent nozzle. There are three injection situations, corresponding to different induction zone back pressures  $p_w$ :

- (1) for  $p_w \geq p_{st}$ , there is no inflow and no source term;
- (2) for  $p_{st} > p_w > p_{cr}$ , the inflow is not choked, thus  $p_i = p_w$ , and.

$$T_i = T_{st} \left( \frac{p_i}{p_{st}} \right)^{\frac{\gamma_R - 1}{\gamma_R}}, \quad (1)$$

$$v_i = \sqrt{\frac{2\gamma_R}{\gamma_R - 1} R_R T_{st} \left[ 1 - \left( \frac{p_i}{p_{st}} \right)^{\frac{\gamma_R - 1}{\gamma_R}} \right]}; \quad (2)$$

(3) for  $p_w \leq p_{cr}$ , the inflow is injected at the critical sonic condition,  $p_i = p_{cr}$ , so.

$$p_i = p_{cr} = p_{st} \left( \frac{2}{\gamma_R + 1} \right)^{\frac{\gamma_R - 1}{\gamma_R}}, \quad (3)$$

where  $\gamma_R$  and  $R_R$  are the average specific heat ratio and gas constant of the detonation products, respectively.

Two parameters are necessary to define the position and angle of the hot jet. The hot jet position is  $K^* L_{in}$  away from the wedge tip, and the jet width  $d$  is fixed at 2 mm in this study. As shown in Fig. 2, the hot jets are injected into the induction zone at jet angle  $\delta$ , which varies from 10° to 90° in this work. The variables and constants used in the simulation are listed in Table 1. The control variables selected in this study are the jet angle  $\delta$ , jet position parameter  $K$ , and flight Mach number  $M_1$ . The wedge angle  $\theta_1$  is fixed at 19°, equivalent to the inflow angle shown in Fig. 2. In other words, the coordinates of the computational domain are rotated to align with the wedge surface in the simulation code.

## 2.2. Numerical methods

Viscous effects have been thought to be negligible in previous detonation studies [17,39,40] because of the high Reynolds numbers of these flows. Many successful ODW studies [31,41–43] are based on the inviscid assumption. Recent investigations [44–47] have explored the influences of viscous boundary layers or turbulence models on ODW structure. Although viscous boundary layers could influence the ODW initiation position, the effects on the main ODW flow region are weak and limited. Overall, the basic flow laws of viscous ODWs have not been systematically clarified. The two-dimensional multi-species Euler equations are used as the governing equations in this investigation to compare with previous research focusing on hot jet effects:

$$\frac{\partial \mathbf{U}}{\partial t} + \frac{\partial \mathbf{F}}{\partial x} + \frac{\partial \mathbf{G}}{\partial y} = \mathbf{S}, \quad (4)$$

where,

$$\mathbf{U} = \begin{bmatrix} \rho_1 \\ \vdots \\ \rho_n \\ \rho u \\ \rho v \\ e \end{bmatrix}, \mathbf{F} = \begin{bmatrix} \rho_1 u \\ \vdots \\ \rho_n u \\ \rho u^2 + p \\ \rho u v \\ (e + p)u \end{bmatrix}, \mathbf{G} = \begin{bmatrix} \rho_1 v \\ \vdots \\ \rho_n v \\ \rho u v \\ \rho v^2 + p \\ (e + p)v \end{bmatrix}, \mathbf{S} = \begin{bmatrix} \omega_1 \\ \vdots \\ \omega_n \\ 0 \\ 0 \\ 0 \end{bmatrix}. \quad (5)$$

Here,  $\rho$ ,  $u$ ,  $v$ , and  $p$  represent the density, velocity along the  $x$ -direction, velocity along the  $y$ -direction, and pressure, respectively. The density  $\rho$  and the total energy  $e$  are calculated from.

$$\rho = \sum_{i=1}^n \rho_i \quad (6)$$

and.

$$e = \rho h - p + \frac{1}{2} \rho (u^2 + v^2), \quad (7)$$

where  $h$  is the specific enthalpy, equal to  $\sum_{i=1}^n \rho_i h_i / \rho$ . Here, the  $h_i$  are the enthalpies calculated from the thermodynamic data for each species. The equation of state for this process is.

$$p = \sum_{i=1}^n \rho_i \frac{R_0}{W_i} T, \quad (8)$$

where  $W_i$  is the molecular weight of the  $i$ -th species,  $T$  is the gas temperature,  $R_0$  is the universal gas constant, and  $\omega_i$  is the mass-based rate at which the  $i$ -th species is produced, determined by the chemical reaction model. The chemical reaction model in this investigation is a comprehensive H<sub>2</sub>/O<sub>2</sub> kinetic mechanism suitable for high-pressure combustion [48] involving 27 reversible, elementary reactions among eight species (H<sub>2</sub>, O<sub>2</sub>, H<sub>2</sub>O, H, O, OH, HO<sub>2</sub>, and H<sub>2</sub>O<sub>2</sub>) in the presence of five inert species (N<sub>2</sub>, Ar, He, CO, and CO<sub>2</sub>). The thermodynamic properties of the chemical species are evaluated using the nine-coefficient NASA polynomial representations [49]. The governing equations are discretized on Cartesian uniform grids and solved using the DCD (Dispersion Controlled Dissipation) scheme [50] with Strang's splitting. Sufficient sub-reaction steps are incorporated to ensure the overall accuracy of the simulation results, overcoming the stiffness problem associated with solving the detailed chemical reaction processes.

The computational domain is shown in Fig. 2. The left and upper boundaries of the computational domain use supersonic inflow conditions determined by the flight conditions and forebody compression process. The post-compression parameters can be obtained from shock-deflection angle relations [27,31,51] using the standard atmospheric parameters at 30 km [52] and the flight Mach number  $M_1$ . The outflow conditions adopted at the right boundary are extrapolated from the interior, assuming zero first-order derivatives. Slip boundary conditions are used on the wedge surface, while the jet region on the wedge employs the inflow condition discussed in Sec. 2.1. The CFD code is verified by comparison with theoretical and experimental results and by grid resolution studies, which are given in the Appendix.

In this study, the flight altitude is fixed to 30 km, and the flight Mach number  $M_1$  varies from 8.0 to 9.5. A homogeneous stoichiometric hydrogen-air mixture with H<sub>2</sub>:O<sub>2</sub>:N<sub>2</sub> = 2:1:3.76 is adopted in all cases. The entire computational domain is initialized with a uniform density, velocity, and pressure specific to the flight conditions and the wedge angle  $\theta$ . The simulations continue until the ODW flow fields converge to a steady state. After the initial ODWs stabilize, the jet flow is activated to study its effects on the ODWs.

**Table 2**

Post-compression inflow and hot jet parameters.

$M_1$	8.0	8.5	9.0	9.5
$p_3$ (kPa)	32.5	37.3	42.5	48.2
$T_3$ (K)	742.8	795.7	851.5	910.3
$V_3$ (m/s)	2188.2	2330.9	2473.4	2615.6
$L_{in}$ (mm)	99.6	53.0	30.7	19.0
$p_{st}$ (kPa)	721.0	1003.3	1315.3	1803.7
$T_{st}$ (K)	3545.4	3752.8	3930.1	4109.1

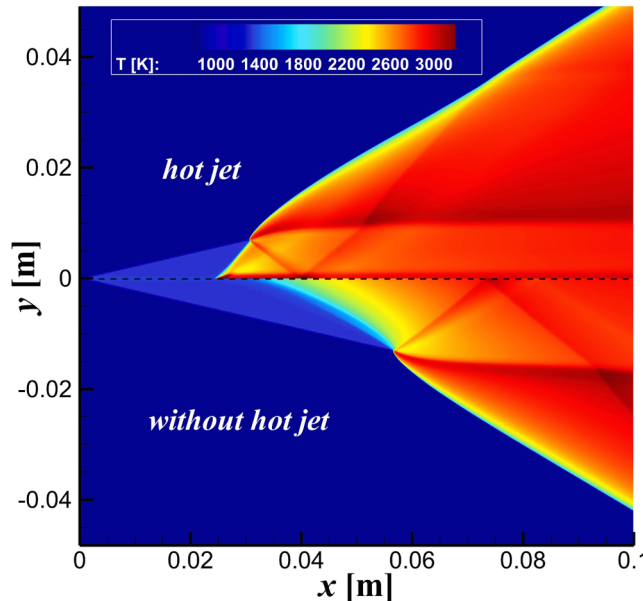


**Fig. 3.** Temperature fields of ODWs with a hot jet (upper) and without a hot jet (lower) for  $M_1 = 9.0$ ,  $K = 0.8$ , and  $\delta = 10^\circ$ .

### 3. Results and discussion

#### 3.1. Initiation with different Mach numbers

The parameters used in the simulations are listed in **Table 2**. As mentioned in the last section, the inflow parameters are first calculated from the shock relation. Next, the ODWs without a jet are simulated, providing the jet parameters  $p_{st}$ ,  $T_{st}$  and initiation length  $L_{in}$  of the original ODWs. The quantities  $P_3$ ,  $T_3$ , and  $V_3$  represent the inflow parameters before detonation, determined by the flight number  $M_1$  and the forebody compression process. As  $M_1$  increases, the inflow parameters ( $P_3$ ,  $T_3$ ,  $V_3$ ) and post-detonation parameters ( $p_{st}$ ,  $T_{st}$ ) increase accordingly while  $L_{in}$  decreases. The detonation flow field with a hot jet can then be simulated using these parameters.

**Fig. 3** shows the original ODW and jet-initiation ODW for  $M_1 = 9.0$ . The jet parameters  $K$  and  $\delta$  are 0.8 and  $10^\circ$ , respectively. Compared with the ODW without a hot jet, the initiation position of the ODW moves upstream after the jet is introduced. The oblique shock-detonation transition originally occurs near  $x = 0.06$  m, moving to approximately  $x = 0.03$  m after the jet is added. A high-temperature region can be observed near the wedge in the upper part of **Fig. 3**, indicating the jet's effect on the temperature field. The ignition occurs just before the jet's injection on the wedge, demonstrating that the jet plays a vital role in the initiation.

**Fig. 4** shows the local wave structure through zoomed temperature and pressure fields to analyze the mechanism of jet-initiated ODWs. Because of the high velocity behind the oblique shock wave induced by the wedge (OSW1), the hot jet is injected into the main flow at a certain angle, as shown by the streamlines in **Fig. 4(c)**. The jet induces a gaseous wedge, generating another oblique shock (OSW2) to instantaneously initiate the detonation and compressing the mixture again to make it detonate further upstream. **Fig. 4(d)** demonstrates the pressure lines along  $y = 0$  m and  $y = 0.003$  m. The pressure variation reflects the shock intensity, indicating that OSW2 is so strong compared to OSW1 that it triggers the mixture directly, which is the physical mechanism of ODW initiation by the hot jet.

We have simulated other cases and observed similar ODWs in which

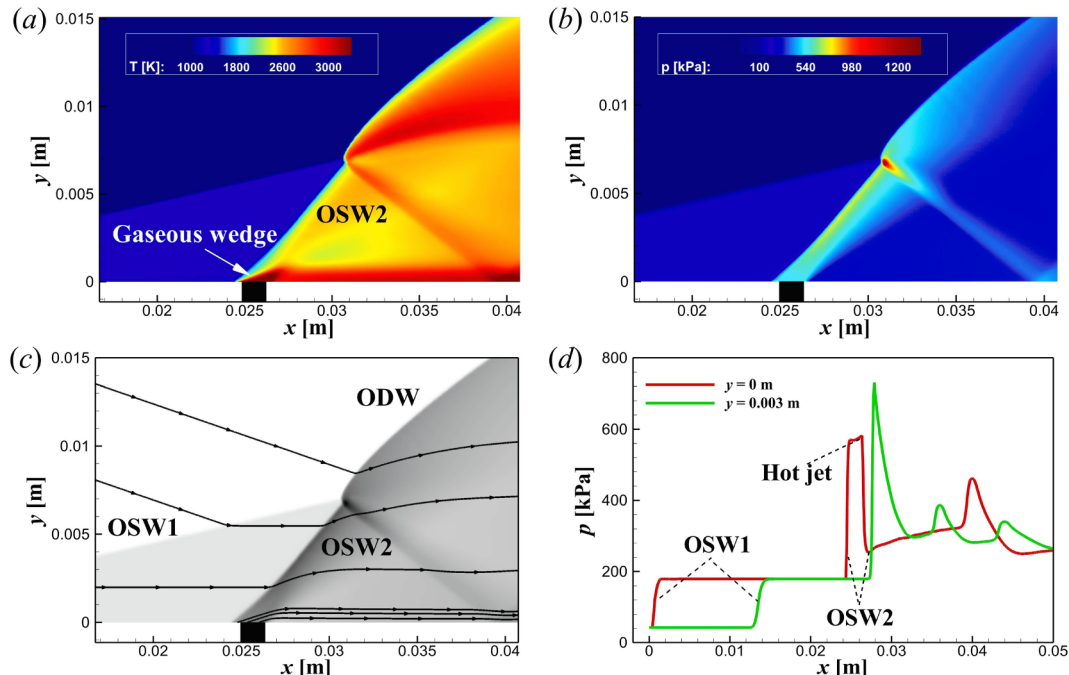


**Fig. 4.** (a) Temperature and (b) pressure fields of a wave structure controlled by a hot jet. (c) Schematic of a local flow field and (d) pressure along different lines parallel to the  $x$ -axis for  $M_1 = 9.0$ .

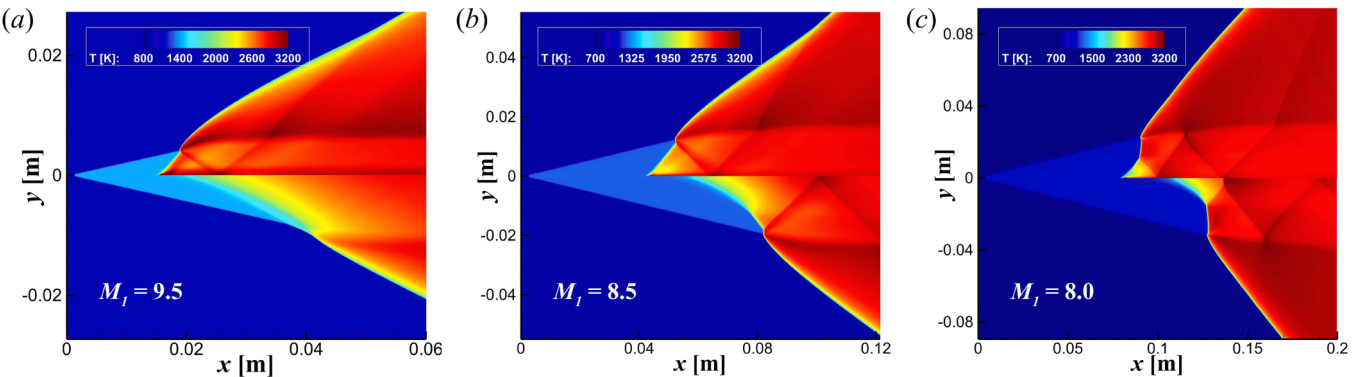


Fig. 5. ODW temperature fields with a hot jet (upper) and without a hot jet (lower) for (a)  $M_1 = 9.5$ ; (b)  $M_1 = 8.5$ ; (c)  $M_1 = 8.0$ .

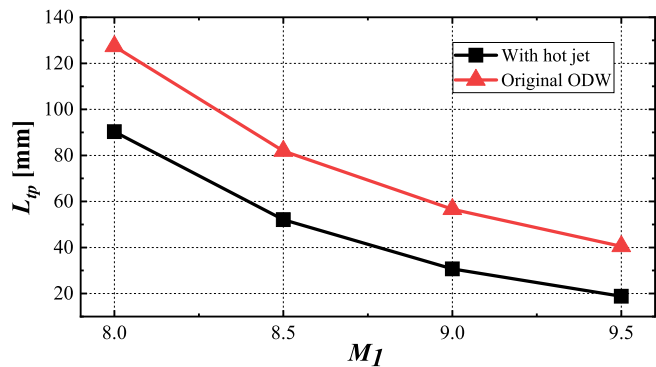


Fig. 6. Triple wave position  $L_{tp}$  as a function of flight Mach number with and without a hot jet.

**Table 3**  
Average pressure recovery coefficient  $\bar{\sigma}$  with and without a hot jet.

$M_1$	$\bar{\sigma}_{O-ODW}$	$\bar{\sigma}_{HJ}$
8.0	0.280	0.282
8.5	0.271	0.278
9.0	0.268	0.274
9.5	0.268	0.281

the jet initiated the ODWs instantaneously by changing the flight Mach number. The effect of the hot jet on the OSW–ODW transition type is notable in Fig. 5(a). After the gas injection, the original ODW with a smooth transition transforms into an abrupt transition structure. This phenomenon can be attributed to the influence of OSW2, induced by the gaseous wedge, which causes the ODW with the hot jet transition to be generally abrupt. In the case of  $M_1 = 8.0$ , a particular structure featuring close-to-normal detonation arises. This structure is nearly unchanged after the jet is introduced, except for the upstream movement of the initiation region.

Fig. 6 compares the triple wave position of the original ODW to that of the ODW with a hot jet as a function of flight Mach number. Compared with the original ODWs, the positions of the triple wave points with jet control are significantly shorter. With or without jet initiation,  $L_{tp}$  follows nearly the same trend as  $M_1$  increases. Together, these results demonstrate that introducing a jet in the induction zone is an effective method to control the initiation position. The transition of jet-controlled ODWs is usually abrupt because of the strong OSW generated by the jet.

However, the effect of the jet on the ODW combustion efficiency is also an important issue, which further affects the thrust performance of the engine. Because the engine outlet model or nozzle is not included, we use the post-combustion total pressure recovery coefficient  $\sigma$  as the

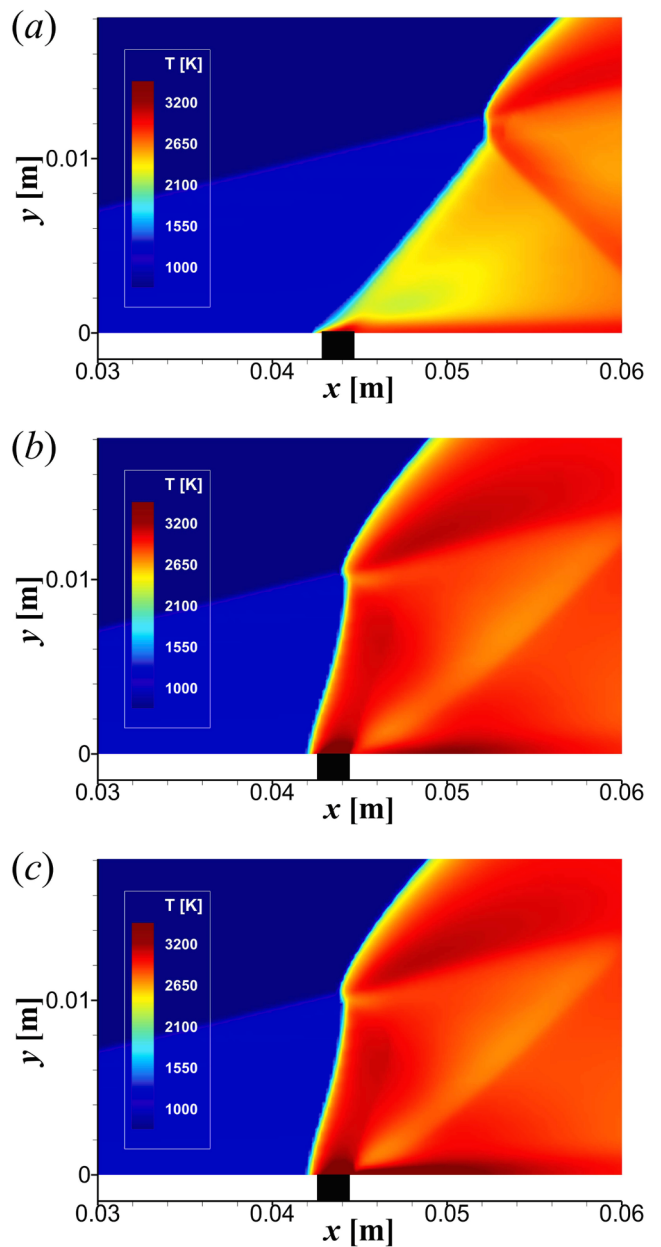


Fig. 7. Temperature fields for a hot-jet-controlled ODW for  $M_1 = 8.5$  and  $K = 0.8$ : (a)  $\delta = 10^\circ$ ; (b)  $\delta = 50^\circ$ ; (c)  $\delta = 90^\circ$ .

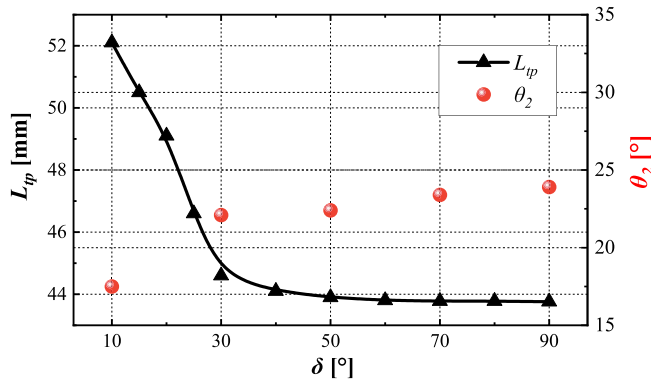


Fig. 8. Triple wave position  $L_{tp}$  and gaseous wedge angle  $\theta_2$  as functions of jet angle  $\delta$  for  $M_1 = 8.5$ .

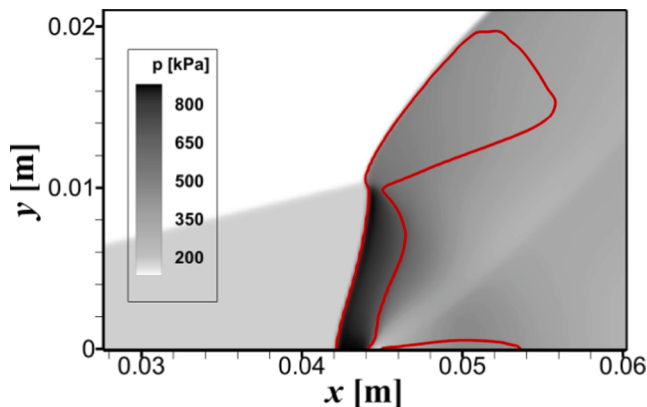


Fig. 9. Pressure fields with red sonic lines of a hot-jet-controlled ODW for  $M_1 = 8.5$ ,  $K = 0.8$ , and  $\delta = 90^\circ$ .

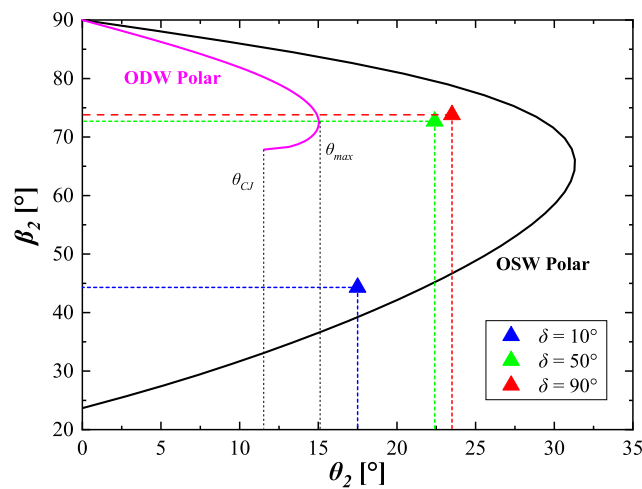


Fig. 10. Polar curve analysis for different jet angles.

key parameter in the engine impulse potential, as proposed in our recent work [27].  $\sigma$  is calculated through dividing the local total pressure by the total pre-combustion pressure, and  $\bar{\sigma}$  is the average value for the ODW outlet section, whose height is twice the initiation region height. Table 3 shows the comparison of  $\bar{\sigma}$  values between the jet-controlled ODW and original ODW, denoted as  $\bar{\sigma}_{HJ}$  and  $\bar{\sigma}_{O-ODW}$ . The results show that  $\bar{\sigma}_{HJ}$  is slightly higher than  $\bar{\sigma}_{O-ODW}$  at different Mach numbers, indicating that jet-controlled ODWs have a higher combustion efficiency

and a greater potential thrust performance.

### 3.2. Effects of jet angle

Because the ODW initiation length is usually too large at relatively low flight Mach numbers and the jet-initiation method is more practical for this situation,  $M_1 = 8.5$  and 8.0 are selected to study the effects of jet angle and jet position. The effects of jet angle are investigated by simulating two other cases,  $\delta = 50^\circ$  and  $90^\circ$ , and comparing them with the default case,  $\delta = 10^\circ$ . The temperature fields with  $M_1 = 8.5$  and  $K = 0.8$  are displayed in Fig. 7 for different jet angles, where the black squares represent the jet region. There is a significant change when the jet angle  $\delta$  is increased to  $50^\circ$ : the high-temperature region near the wedge in the case of  $\delta = 10^\circ$  can no longer be easily observed, and the OSW2 angle is significantly increased. Meanwhile, the triple wave position is correspondingly close to the upstream. As the jet angle  $\delta$  rises to  $90^\circ$ , the ODW structure and initiation position are almost unchanged compared to those for  $\delta = 50^\circ$ , revealing that the ODW structure is insensitive to jet angle when  $\delta$  is above  $50^\circ$ .

The triple wave position  $L_{tp}$  and gaseous wedge angle  $\theta_2$  are plotted for different jet angles  $\delta$  in Fig. 8 to explain why the flow fields are similar when  $\delta$  is above  $50^\circ$ . Consistent with the phenomenon described above, the triple wave position  $L_{tp}$  remains at about 44 mm when  $\delta$  exceeds  $50^\circ$ , rather than continuously decreasing with increasing jet angle. This effect is attributed to the invariance of  $\theta_2$  induced by the hot jet, shown as the red dots in Fig. 8. This is a very interesting phenomenon because a larger jet angle implies increased jet strength, but the actual gaseous wedge angle remains the same with the increase in jet angle.

To further explain why the gaseous wedge angle becomes constant, Fig. 9 presents pressure fields with red sonic lines for  $\delta = 90^\circ$ . The most interesting aspect of this image is the high-pressure and subsonic zone behind OSW2, indicating that OSW2 is a strong OSW solution according to polar theory [53]. Fig. 10 shows the theoretical shock and detonation polar curves obtained with the induction zone parameters, where  $\theta_2$  represents the angle of the gaseous wedge, and  $\beta_2$  represents the wave angle of OSW2 or ODW2. The triangular scatter points are the numerical simulation results, representing the angles of the gaseous wedge and induced OSW2. For the case of  $\delta = 10^\circ$ , the numerical result is located near the lower half of the shock polar curve, which is consistent with the OSW structure induced by the gaseous wedge in the flow field. For the cases of  $\delta = 50^\circ$  and  $90^\circ$ , there is a secondary ODW below the triple points. According to the theoretical detonation polar curve,  $\theta_2$  is larger than the maximum wedge angle  $\theta_{max}$  of the attached detonation wave, indicating the ODW2 is a detached detonation wave for the gaseous wedge. However, because the local inflow velocity is still higher than the velocity of the corresponding Chapman–Jouguet detonation, ODW2 remains stable at the end of the induction zone. This stronger ODW2 leads to a higher pressure in the jet region. According to the sonic injection model, the actual jet strength is weakened to match the back pressure, i.e., situation (2) mentioned in Sec. 2.1, providing the physical explanation for the limited effects of the large jet angle on ODW initiation. These effects of the induction zone flow on the gas injection have not been reported in previous research on jet-controlled ODWs and are a meaningful consideration for engine applications.

### 3.3. Effects of jet position

The jet position is another critical parameter that has been set at  $0.8L_{in}$  ( $K = 0.8$ ) in the above cases. In practical application of ODEs, some small jet holes can be set on the wedge, and the jet position can be adjusted by opening/closing the jet holes. To investigate the effects of  $K$ , three additional cases,  $K = 0.6$ , 0.4, and 0.2, are simulated. Considering the baseline case of  $M_1 = 8.0$  has a special structure with an NDW below the triple wave point and may be more sensitive to jet position, cases of  $M_1 = 8.0$  are first selected and shown in Fig. 11. As the jet position gradually approaches the front tip of the wedge, a particular structure

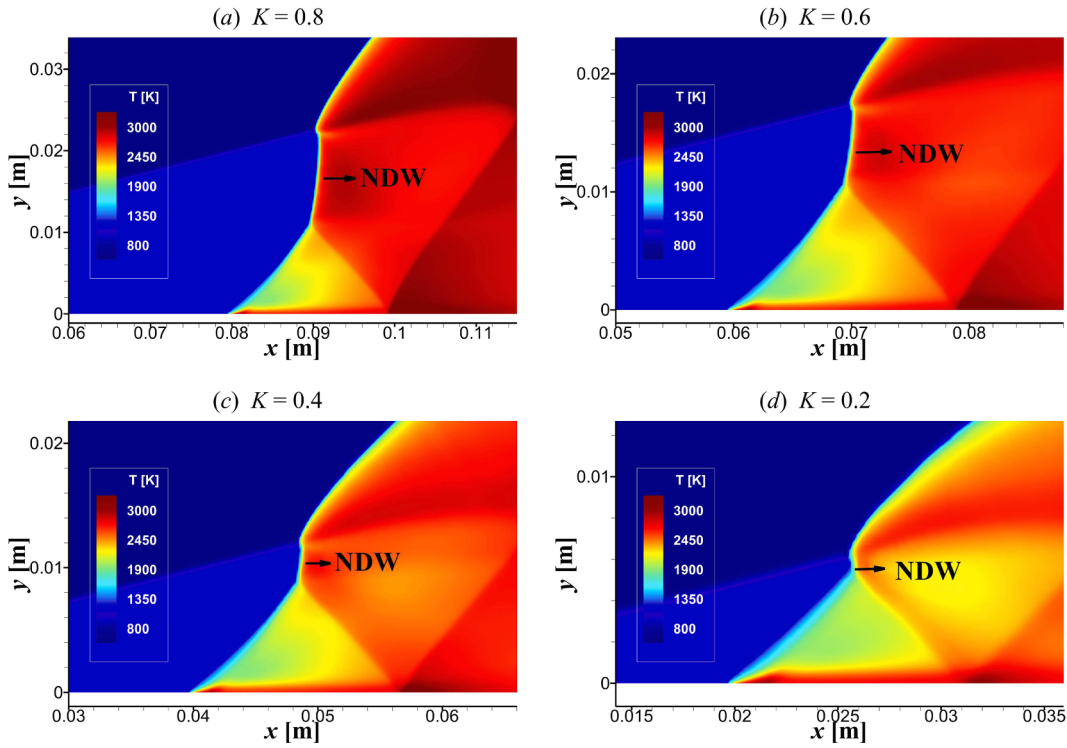


**Fig. 11.** Temperature fields of hot-jet-controlled ODWs with  $M_I = 8.0$  and  $\delta = 10^\circ$ : (a)  $K = 0.8$ ; (b)  $K = 0.6$ ; (c)  $K = 0.4$ ; (d)  $K = 0.2$ .

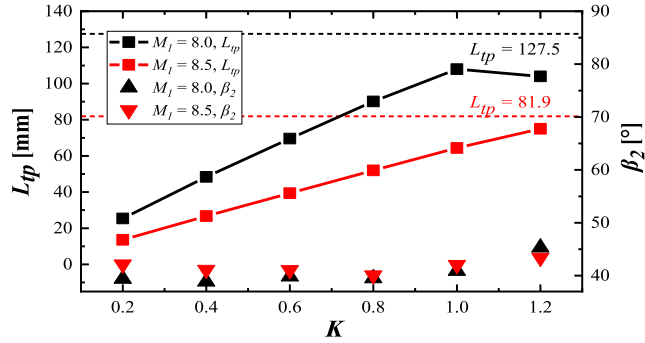


**Fig. 12.** Triple wave position  $L_{tp}$  and gaseous wedge angle  $\beta_2$  as functions of jet position parameter  $K$  for  $M_I = 8.5$  and  $M_I = 8.0$ .

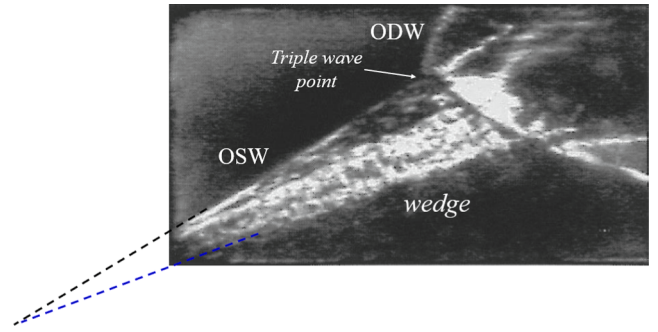


**Fig. A1.** Schlieren image of the flow field obtained by Viguerie et al [55].

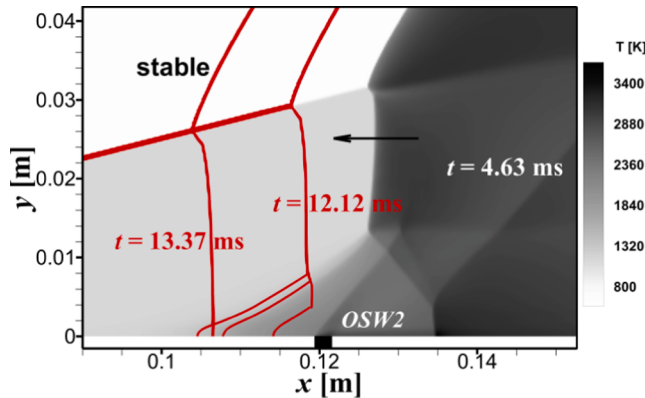


**Fig. 13.** Temperature field and shock front at different instants (red curves) for  $M_I = 8.0$ ,  $\delta = 10^\circ$ , and  $K = 1.2$ .

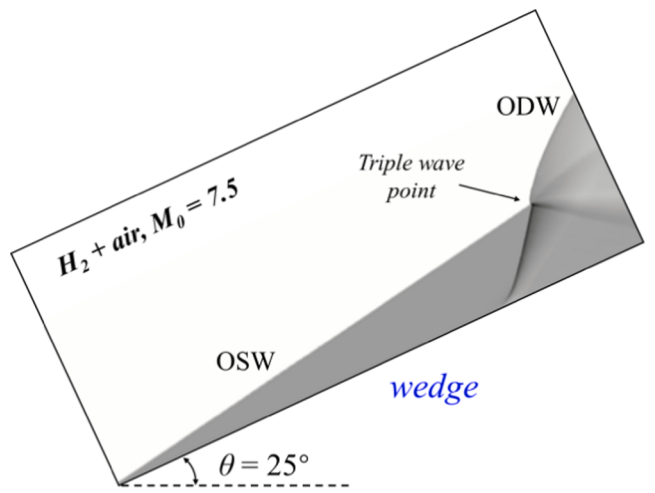


**Fig. A2.** Density fields simulated by our own code.

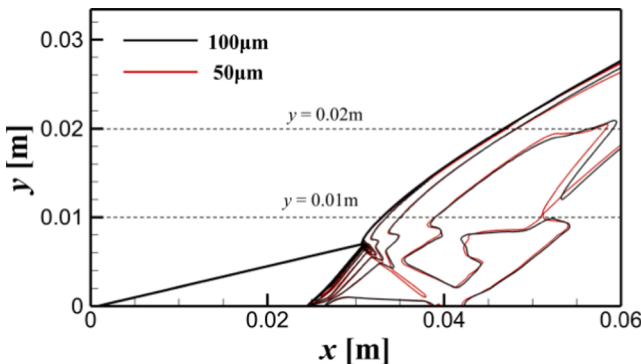


Fig. A3. Density fields with different grid scales for  $M_1 = 9.0$ .

featuring close-to-normal detonation near the triple wave point still exists. The height of the normal detonation becomes shorter with decreasing  $K$ , although the OSW2 angle is nearly constant. This trend can be attributed to the height of the compression waves and induction zone [31,54]. For different jet positions,  $H_{CW}$  is similar, but  $H_{ini}$  decreases as  $K$  varies. This geometric difference results in variations in the ODW morphology with the movement of the jet position.

Additional cases are simulated to investigate the effect of jet position on initiation distance. The relationships of  $L_p$  and the gaseous wedge angle  $\beta_2$  to  $K$  for  $M_1 = 8.0$  and 8.5 are displayed in Fig. 12, where the dashed line represents the triple wave position of each original ODW, the solid lines show the triple wave position  $L_p$ , and the triangular scatter points represent the gaseous wedge angle. These results prove once again that a jet can effectively shorten the initiation length. Except for the case of  $K = 1.2$  and  $M_1 = 8.0$ ,  $L_p$  increases linearly with jet position  $K$ , indicating that a strong jet can achieve instantaneous initiation. This linear relationship can be explained by the angle of OSW2,  $\beta_2$ , which remains almost the same owing to the fixed jet angle, although the jet position is varied. This linear relation is conducive to precise control of ODW initiation in engineering applications.

$L_p$  decreases when  $K = 1.2$  and  $M_1 = 8.0$  because the jet drives the ODW upstream. Fig. 13 shows the temperature field and shock front of this unique case at different times (red curves). Initially, the OSW induced by the hot jet is introduced to the initiation zone, destabilizing the original wave configuration and causing the ODW to travel upstream. In the later stages, the oblique wave near the wedge disappears gradually on a time scale of  $10^{-3}$  s. Eventually, the initiation zone evolves into only one shock perpendicular to the wedge at 13.37 ms. It should be noted that this structure remains stable because the local inflow velocity remains higher than the velocity of the corresponding Chapman–Jouguet detonation. This stable result is consistent with the  $M_S / M_{CJ}$  criterion proposed in our previous research [28].

#### 4. Conclusion

ODWs with and without jets have been simulated and compared in this study for application to oblique detonation engines. The Euler equation was used with detailed chemical and sonic injection models. The main conclusions are as follows:

1. A hot jet is an effective method to control the initiation position. For situations of large initiation length caused by a low flight Mach number and a high-altitude or low-density atmosphere, this jet-controlled method may broaden the engine's working range of flight speeds and altitudes.
2. Jet-controlled ODWs are triggered by a gaseous wedge that generates a strong oblique shock to ignite the mixture instantaneously. Because of this initiation mechanism, the transition zone of jet-controlled ODWs is usually the abrupt type. Furthermore, introducing a hot jet can slightly reduce the total pressure loss of the detonation process, which helps improve thrust performance.
3. The jet angle is a critical parameter for controlling ODWs. When the jet angle is large, a strong solution of secondary oblique detonation may appear in the initiation zone, weakening the jet and making the ODWs insensitive to the jet angle.
4. ODWs are sensitive to jet position. A strong jet can achieve an instantaneous initiation, so the ignition length varies linearly with jet position. If the jet is in the initiation zone, the shock induced by the gaseous wedge may drive the ODWs upstream. However, the stability of the overall wave configuration is independent of the hot jet.

Many key issues for promoting practical application of ODEs are not covered by this article. These include how to mix fuel with the

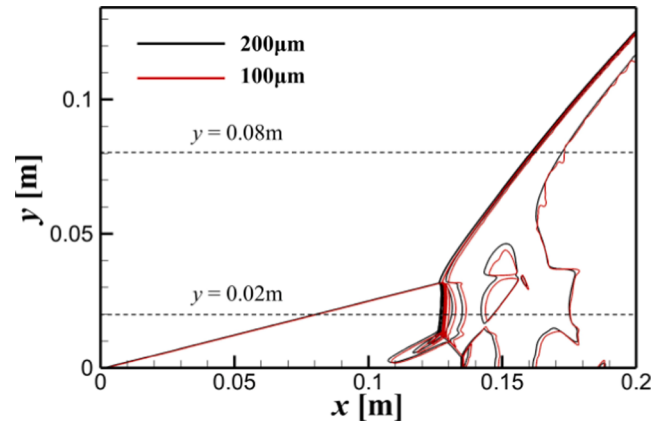


Fig. A5. Density fields with different grid scales for  $M_1 = 8.0$ .

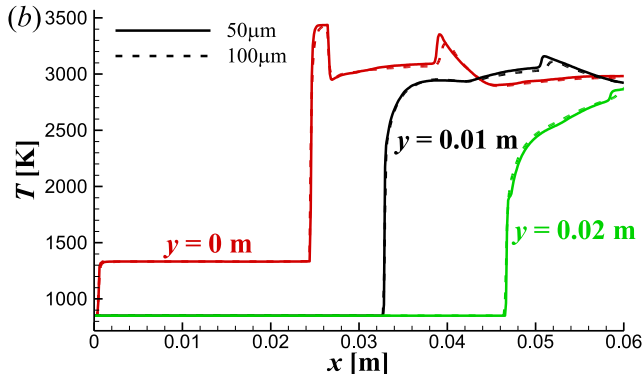
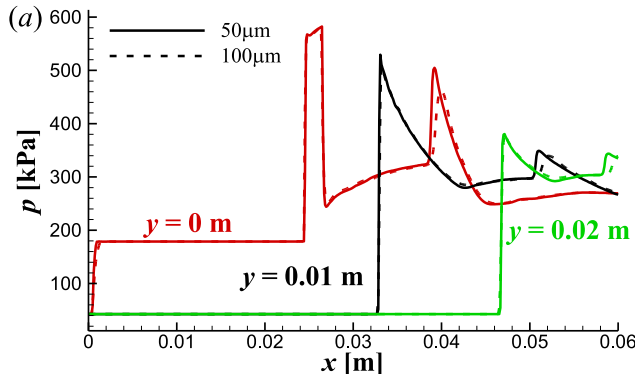
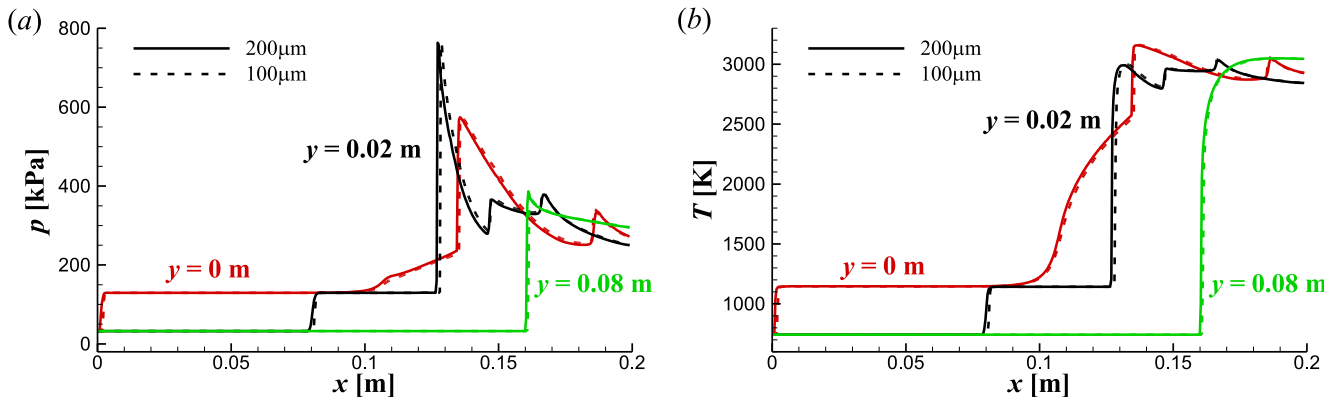


Fig. A4. Pressure and temperature along different lines parallel to the  $x$ -axis with different grid scales for  $M_1 = 9.0$ .



**Fig. A6.** Pressure and temperature along different lines parallel to the  $x$ -axis with different grid scales for  $M_1 = 8.0$ .

supersonic air sufficiently and quickly, and how to control the ODWs in the combustor with a wide range of flight conditions. Because an ODE does not have self-starting ability, it is also important to explore combined power. Further advancing engineering application of ODEs requires more systematic research on overall aircraft engine technology in the future.

#### Declaration of Competing Interest

The authors declare that they have no known competing financial interests or personal relationships that could have appeared to influence the work reported in this paper.

#### Acknowledgement

This research was supported by the National Natural Science Foundation of China (NSFC Nos. 11972331; 12002041; 11822202). We thank Robert A. Brewster, PhD, from Liwen Bianji (Edanz) for editing a draft of this manuscript.

#### Appendix

To verify the simulation code, the validations are conducted by comparing with the experimental results obtained by Viguier et al [55], as shown in Fig. A1. The initial conditions are consistent with the experiments, i.e. the temperature and pressure before the ODW are 293 K and 0.4 bar. Fig. A2 shows the density fields simulated by the CFD code. The basic ODW structures such as the OSW, ODW, and triple wave points appear in both the experimental and numerical results, and the overall fields are very similar. The numerical angles of the OSW and ODW are  $8.32^\circ$  and  $45.0^\circ$  respectively, which are consistent with the theoretical values according to polar analysis ( $8.16^\circ$  and  $44.6^\circ$ ). These comparisons prove that the CFD code used in this paper can simulate the basic ODW structure reliably. Furthermore, we have conducted a lot of verification and assessment of this CFD code in our previous work [27,28,51], indicating it has a high credibility.

Meanwhile, it is necessary to exclude the influence of grid size on the simulation results. Because the present cases cover a wide range of flight conditions for ODEs, both the physical length of the induction zone and the heat release rate vary in a large range corresponding to different values of the flight Mach number  $M_1$ . The flow scale and chemical reaction scale increase as the flight Mach number decreases. Considering rational allocation of computing resources, the grid size varies from 100  $\mu\text{m}$  to 200  $\mu\text{m}$  for different cases. To ensure that the simulation results are independent of the mesh size, grid resolution studies are conducted by comparing numerical results after doubling the number of grids in the computational domain in both the  $x$ - and  $y$ -directions. Fig. A3 shows the density isolines for  $M_1 = 9.0$ ,  $K = 0.8$ , and  $\delta = 10^\circ$

with the default mesh size of 100  $\mu\text{m}$  compared with the simulation results obtained by a finer mesh size of 50  $\mu\text{m}$ . There is almost no difference between the two wave structures for the two grid length scales. As further verifications, quantitative comparisons of the pressure and temperature along three parallel lines are provided in Fig. A4. The curves are nearly coincident for the hot jet and shock positions, indicating that the default mesh size of 100  $\mu\text{m}$  is sufficient to capture the fine ODW structures of this case. The 200- $\mu\text{m}$  grid size is also verified by comparison with the simulation results for 100  $\mu\text{m}$ . Fig. A5 and Fig. A6 show the density field isolines and pressure and temperature lines for Mach 8.0 with a mesh size of 200  $\mu\text{m}$  compared with the result obtained with 100  $\mu\text{m}$ . Both the density fields and quantitative curves show very similar ODW structures between 200  $\mu\text{m}$  and 100  $\mu\text{m}$ , indicating the mesh size of 200  $\mu\text{m}$  is capable of capturing the fine ODW structures for  $M_1 = 8.0$ . Similar grid resolution studies have been conducted for other cases, ensuring that the results presented in this investigation are independent of grid size.

#### References

- [1] K. Kailasanath, Review of propulsion applications of detonation waves, *AIAA J.* 38 (2000) 1698–1708.
- [2] P. Wolański, Detonative propulsion, *Proc. Combust. Inst.* 34 (2013) 125–158.
- [3] Q. Zhang, X. Qiao, W. Fan, K. Wang, F. Tan, J. Wang, Study on operation and propulsion features of a pulse detonation rocket engine with secondary oxidizer injection, *Appl. Therm. Eng.* 180 (2020) 115661.
- [4] B. Zhang, Y. Li, H. Liu, Analysis of the ignition induced by shock wave focusing equipped with conical and hemispherical reflectors, *Combust. Flame* 236 (2022), 111763.
- [5] M. Zhao, Z. Ren, H. Zhang, Pulsating detonative combustion in n-heptane/air mixtures under off-stoichiometric conditions, *Combust. Flame* 226 (2021) 285–301.
- [6] D. Kublik, J. Kindracki, P. Wolański, Evaluation of wall heat loads in the region of detonation propagation of detonative propulsion combustion chambers, *Appl. Therm. Eng.* 156 (2019) 606–618.
- [7] J. Wang, W. Lin, W. Huang, Q. Shi, J. Zhao, Numerical study on atomization and evaporation characteristics of preheated kerosene jet in a rotating detonation scramjet combustor, *Appl. Therm. Eng.* 203 (2022), 117920.
- [8] M. Zhao, H. Zhang, Rotating detonative combustion in partially pre-vaporized dilute n-heptane sprays: Droplet size and equivalence ratio effects, *Fuel* 304 (2021), 121481.
- [9] D.A. Rosato, M. Thornton, J. Sosa, C. Bachman, G.B. Goodwin, K.A. Ahmed, Stabilized detonation for hypersonic propulsion, *Proc Natl Acad Sci U S A* 118 (2021) 1–7.
- [10] G. Zhang, G. Li, K. Wang, Wave structure of oblique detonation disturbed by an expansion wave from a bended tunnel, *Appl. Therm. Eng.* 180 (2020), 115856.
- [11] Q. Qin, X. Zhang, A novel method for trigger location control of the oblique detonation wave by a modified wedge, *Combust. Flame* 197 (2018) 65–77.
- [12] Z. Zhang, C. Wen, W. Zhang, Y. Liu, Z. Jiang, Formation of stabilized oblique detonation waves in a combustor, *Combust. Flame* 223 (2021) 423–436.
- [13] M.V. Papalexandris, A Numerical Study of Wedge-Induced Detonations, *Combust. Flame* 120 (4) (2000) 526–538.
- [14] H.H. Teng, Z.L. Jiang, On the transition pattern of the oblique detonation structure, *J. Fluid Mech.* 713 (2012) 659–669.
- [15] H. Teng, Z. Jiang, Progress in multi-wave structure and stability of oblique detonations, *Adv. Mech.* 50 (2020), 202002.

- [16] C. Li, K. Kailasanath, E.S. Oran, Detonation structures behind oblique shocks, *Phys. Fluids* 6 (4) (1994) 1600–1611.
- [17] L. Fernando, F. Silva, B. Deshaies, Stabilization of an Oblique Detonation Wave by a Wedge: A Parametric Numerical Study, *Combust. Flame* 121 (2000) 152–166.
- [18] W. Han, C. Wang, C.K. Law, Three-dimensional simulation of oblique detonation waves attached to cone, *Phys. Rev. Fluids* 4 (2019), 053201.
- [19] Y. Fang, Z. Zhang, Z. Hu, X. Deng, Initiation of oblique detonation waves induced by a blunt wedge in stoichiometric hydrogen-air mixtures, *Aerosp. Sci. Technol.* 92 (2019) 676–684.
- [20] K. Ghorbanian, J.D. Sterling, Influence of formation processes on oblique detonation wave stabilization, *J. Propul. Power* 12 (1996) 509–517.
- [21] S. Bhatrai, H. Tang, Formation of near-Chapman-Jouguet oblique detonation wave over a dual-angle ramp, *Aerosp. Sci. Technol.* 63 (2017) 1–8.
- [22] H. Teng, Y. Zhang, P. Yang, Z. Jiang, Oblique detonation wave triggered by a double wedge in hypersonic flow, *Chin. J. Aeronaut.* 35 (4) (2022) 176–184.
- [23] S. Maeda, R. Inada, J. Kasahara, A. Matsuo, Visualization of the non-steady state oblique detonation wave phenomena around hypersonic spherical projectile, *Proc. Combust. Inst.* 33 (2011) 2343–2349.
- [24] S. Maeda, J. Kasahara, A. Matsuo, Oblique detonation wave stability around a spherical projectile by a high time resolution optical observation, *Combust. Flame* 159 (2012) 887–896.
- [25] J. Verreault, A.J. Higgins, Initiation of detonation by conical projectiles, *Proc. Combust. Inst.* 33 (2011) 2311–2318.
- [26] Z. Zhang, C. Wen, C. Yuan, Y. Liu, G. Han, C. Wang, Z. Jiang, An experimental study of formation of stabilized oblique detonation waves in a combustor, *Combust. Flame* 237 (2022) 111868.
- [27] J. Bian, L. Zhou, H. Teng, Structural and thermal analysis on oblique detonation influenced by different forebody compressions in hydrogen-air mixtures, *Fuel* 286 (2021), 119458.
- [28] H. Teng, J. Bian, L. Zhou, Y. Zhang, A numerical investigation of oblique detonation waves in hydrogen-air mixtures at low mach numbers, *Int. J. Hydrogen Energy* 46 (2021) 10984–10994.
- [29] H. Li, J. Li, C. Xiong, W. Fan, L. Zhao, W. Han, Investigation of hot jet on active control of oblique detonation waves, *Chin. J. Aeronaut.* 33 (2020) 861–869.
- [30] Q. Qin, X. Zhang, Study on the initiation characteristics of the oblique detonation wave by a co-flow hot jet, *Acta Astronaut.* 177 (2020) 86–95.
- [31] H. Teng, C. Tian, Y. Zhang, L. Zhou, H.D. Ng, Morphology of oblique detonation waves in a stoichiometric hydrogen-air mixture, *J. Fluid Mech.* 913 (2021) A1.
- [32] Z. Zhang, K. Ma, W. Zhang, X. Han, Y. Liu, Z. Jiang, Numerical investigation of a Mach 9 oblique detonation engine with fuel pre-injection, *Aerosp. Sci. Technol.* 105 (2020), 106054.
- [33] Z. Ren, B. Wang, G. Xiang, D. Zhao, L. Zheng, Supersonic spray combustion subject to scramjets: progress and challenges, *progress in aerospace science*, 105 (2019) 40–59.
- [34] H. Teng, H.D. Ng, Z. Jiang, Initiation characteristics of wedge-induced oblique detonation waves in a stoichiometric hydrogen-air mixture, *Proc. Combust. Inst.* 36 (2017) 2735–2742.
- [35] Y. Zhang, Y. Fang, H.D. Ng, H. Teng, Numerical investigation on the initiation of oblique detonation waves in stoichiometric acetylene–oxygen mixtures with high argon dilution, *Combust. Flame* 204 (2019) 391–396.
- [36] D. Schwer, K. Kailasanath, Numerical investigation of the physics of rotating-detonation-engines, *Proc. Combust. Inst.* 33 (2011) 2195–2202.
- [37] D. Schwer, K. Kailasanath, Numerical Study of the Effects of Engine Size on Rotating Detonation Engines. 49th AIAA Aerospace Sciences Meeting including the New Horizons Forum and Aerospace Exposition, 2011.
- [38] T.-H. Yi, J. Lou, C. Turangan, J.-Y. Choi, P. Wolanski, Propulsive Performance of a Continuously Rotating Detonation Engine, *J. Propul. Power* 27 (2011) 171–181.
- [39] C. Li, K. Kailasanath, E. Oran, Effects of boundary layers on oblique-detonation structures, in: 31st Aerospace Sciences Meeting (1993).
- [40] L. Deng, H. Ma, C. Xu, X. Liu, C. Zhou, The feasibility of mode control in rotating detonation engine, *Appl. Therm. Eng.* 129 (2018) 1538–1550.
- [41] J.-Y. Choi, D.-W. Kim, I.-S. Jeung, F. Ma, V. Yang, Cell-like structure of unstable oblique detonation wave from high-resolution numerical simulation, *Proc. Combust. Inst.* 31 (2007) 2473–2480.
- [42] J.-Y. Choi, E.J.R. Shin, I.-S. Jeung, Unstable combustion induced by oblique shock waves at the non-attaching condition of the oblique detonation wave, *Proc. Combust. Inst.* 32 (2009) 2387–2396.
- [43] K. Wang, H. Teng, P. Yang, H.D. Ng, Numerical investigation of flow structures resulting from the interaction between an oblique detonation wave and an upper expansion corner, *J. Fluid Mech.* 903 (2020) A28.
- [44] C.L. Bachman, G.B. Goodwin, Ignition criteria and the effect of boundary layers on wedge-stabilized oblique detonation waves, *Combust. Flame* 223 (2021) 271–283.
- [45] Y. Fang, Z. Zhang, Z. Hu, Effects of boundary layer on wedge-induced oblique detonation structures in hydrogen-air mixtures, *Int. J. Hydrogen Energy* 44 (2019) 23429–23435.
- [46] G. Li, G. Zhang, Y. Zhang, L. Ji, S. Gao, Influence of viscous boundary layer on initiation zone structure of two-dimensional oblique detonation wave, *Aerosp. Sci. Technol.* 104 (2020) 106019.
- [47] M. Yu, S. Miao, Initiation characteristics of wedge-induced oblique detonation waves in turbulence flows, *Acta Astronaut.* 147 (2018) 195–204.
- [48] M.P. Burke, M. Chaos, Y. Ju, F.L. Dryer, S.J. Klippenstein, Comprehensive H<sub>2</sub>/O<sub>2</sub> kinetic model for high-pressure combustion, *Int. J. Chem. Kinet.* 44 (2012) 444–474.
- [49] B.J. McBride, M.J. Zehe, S. Gordon, NASA Glenn coefficients for calculating thermodynamic properties of individual species. NASA Glenn Research Center, Cleveland; 2002. Report No.: NASA/TP-2002-211556.
- [50] Z. Jiang, On dispersion-controlled principles for non-oscillatory shock-capturing schemes, *Acta Mech. Sin.* (2004) 1–15.
- [51] T. Wang, Y. Zhang, H. Teng, Z. Jiang, H.D. Ng, Numerical study of oblique detonation wave initiation in a stoichiometric hydrogen-air mixture, *Phys. Fluids* 27 (9) (2015) 096101.
- [52] R. L. King, A computer version of the U. S. Standard Atmosphere, 1976. Science Applications, Inc; 1978. Report No.: NASA-CR-150778.
- [53] H. Teng, H.D. Ng, P. Yang, K. Wang, Near-field relaxation subsequent to the onset of oblique detonations with a two-step kinetic model, *Phys. Fluids* 33 (9) (2021) 096106.
- [54] X. Shi, H. Xie, L. Zhou, Y. Zhang, A theoretical criterion on the initiation type of oblique detonation waves, *Acta Astronaut.* 190 (2022) 342–348.
- [55] C. Viguier, L. Silva, D. Desbordes, B. Deshaies, Onset of oblique detonation waves: Comparison between experimental and numerical results for hydrogen-air mixtures. Symposium (International) on Combustion. Elsevier, 26(1996) 3023–3031.